Quasi-thermal noise measurements on STEREO: Kinetic temperature deduction using electron shot noise model

M. Martinović, A. Zaslavsky, M. Maksimović, N. Meyer-Vernet, S. Šegan, I. Zouganelis, C. Salem, M. Pulupa, S. D Bale

AGU PUBLICATIONS

JGR

Journal of Geophysical Research: Space Physics

TECHNICAL REPORTS: METHODS

10.1002/2015JA021710

Special Section:
Low-Frequency Waves in Space Plasmas

Key Points:
- Quasi-thermal noise spectroscopy is accommodated to S/WAVES instrument
- A survey of the electron temperature on board STEREO A and B is provided
- Obtained results are compared with Wind measurements

Correspondence to:
M. M. Martinović,
mihailo.martinovic@obspm.fr

Citation:
Martinović, M. M., A. Zaslavsky, M. Maksimović, N. Meyer-Vernet, S. Šegan, I. Zouganelis, C. Salem, M. Pulupa, and S. D. Bale (2016), Quasi-thermal noise measurements on STEREO: Kinetic temperature deduction using electron shot noise model, *J. Geophys. Res. Space Physics*, *121*, 129–139, doi:10.1002/2015JA021710.

Received 21 JUL 2015
Accepted 1 DEC 2015
Accepted article online 12 DEC 2015
Published online 6 JAN 2016
Corrected 31 MAY 2016
Corrected 2 AUG 2016

This article was corrected on 31 MAY 2016 and 2 AUG 2016. See the end of the full text for details.

Quasi-thermal noise measurements on STEREO: Kinetic temperature deduction using electron shot noise model

M. M. Martinović[1,2,3], A. Zaslavsky[1], M. Maksimović[1], N. Meyer-Vernet[1], S. Šegan[2], I. Zouganelis[4], C. Salem[5], M. Pulupa[5], and S. D. Bale[5,6]

[1]LESIA, Observatoire de Paris, UPMC, Université Paris Diderot, CNRS, Meudon, France, [2]Department of Astronomy, Faculty of Mathematics, Belgrade, Serbia, [3]IHIS Techno-experts d.o.o. - Research and Development Center, Belgrade, Serbia, [4]European Space Agency, Science and Robotic Exploration Directorate, ESAC, Madrid, Spain, [5]Space Sciences Laboratory, University of California, Berkeley, California, USA, [6]Physics Department, University of California, Berkeley, California, USA

Abstract Quasi-thermal noise (QTN) spectroscopy is an accurate technique for in situ measurements of electron density and temperature in space plasmas. A QTN spectrum is determined by plasma and antenna properties. On STEREO/WAVES, since the antennas are relatively short and thick, the QTN spectrum is dominated by electron shot noise, especially at low frequencies, which reduces the accuracy of the method. Here we use the STEREO low-frequency receiver, proton density measured by Plasma and Suprathermal Ion Composition instrument, and a QTN and shot noise models to provide electron temperature data from both STEREO A and B spacecraft. This derivation is important since no reliable measurements of electron temperature exist on board these spacecraft. We compare the results of our analysis with the electron temperature provided by the Wind spacecraft during the period when Wind and STEREO B were close to each other. The comparison shows that our technique is reliable when results are integrated on a time scale of the order of 50 to 60 min.

1. Introduction

Quasi-thermal noise (QTN) spectroscopy is an accurate technique for in situ measurements of electron density and temperature in space plasmas [*Meyer-Vernet*, 1979]. This technique is based on measurements of the electric field fluctuations induced by the thermal motion of plasma's particles. A QTN spectrum is fully determined by plasma particles' velocity distribution function (VDF) and by the properties of the antennas that measure the electric field fluctuations. This technique is independent of antenna orientation if the VDF of plasma particles is isotropic, and magnetic field is small enough [*Meyer-Vernet*, 1994].

In this work, we apply QTN technique to the Solar Terrestrial Relations Observatory (STEREO) A and B spacecraft in order to obtain electron moments. These measurements are of importance as STEREO Solar Wind Electron Analyzer electron analyzers malfunction in detection of low-energy (below 45 eV) electrons since beginning of the mission and, at present time, no reliable measurements on thermal electrons exist on board these spacecraft [*Fedorov et al.*, 2011]. In general, it is possible to obtain electron local density n_e and kinetic temperature T_e as independent parameters from the analysis of a QTN spectrum. This is due to the existence of a characteristic "plasma peak" just above plasma frequency $f_p = (2\pi)^{-1}\sqrt{n_e e^2/\epsilon_0 m_e}$ (with e and m_e being electron charge and mass, respectively, and ϵ_0 is dielectric permittivity of vacuum). The size and shape of this peak are strongly dependent on the ratio of antenna length L_{ant} to local Debye length L_{D} [*Meyer-Vernet and Perche*, 1989]. A condition for the peak to be clearly visible and therefore for the local density to be directly measurable is that this ratio is greater than 2 or that there is a significant proportion of suprathermal electrons. However, since STEREO is equipped with 6 m monopoles and orbits at 1 AU from the Sun, where local Debye length is of the order of 10 m, the peak is expected to be observed only under special circumstances, e.g., in structures of high density and low temperature where the Debye length is small [*Bougeret et al.*, 2008].

Beside VDF, the QTN spectrum is highly affected by size and shape of the antennas which, on STEREO/WAVES, have a large surface area [*Bale et al.*, 2008]. Particles impacting the antenna produce so-called shot noise [*Meyer-Vernet*, 1983] to appear at lower frequencies. This signal is proportional to the electron impact rate on the antennas surface ($N_{\mathrm{impact}} \sim n_e\sqrt{T_e}$) so that on STEREO it dominates the power spectrum at frequencies

lower than f_p. Therefore, measurement of the product $n_e\sqrt{T_e}$ can be derived from the shot noise spectra. Such kind of measurements have been previously performed by *Zouganelis et al.* [2010] to derive the base capacitance of the STEREO/WAVES dipole. It is important to note that the method described here is impossible to perform when there are dust impacts detected by the dipole, because the signal caused by dust is very high due to large antenna radii [*Pantellini et al.*, 2012] and overwhelms the thermal noise.

Here after describing the details of the QTN spectroscopy technique accommodated for STEREO (section 2), we use STEREO low-frequency receiver (LFR) measurements of the QTN, coupled with proton density measurements by Plasma and Supra-Thermal Ion Composition (PLASTIC) instrument to provide electron temperature data for both STEREO A and B spacecraft (section 3). The data from PLASTIC were used for both obtaining proton parameters and electron density estimate, so electron temperature could be measured independently.

Finally, due to lack of electron analyzers data to use for calibration, we compare the results of our analysis with the electron temperature provided by Wind spacecraft by using data from the period when Wind and STEREO B were positioned close to each other (section 4). This comparison shows that our technique is reliable when integrated on a timescale of the order of 50 to 60 min. Electron temperature histograms accumulated over 10 months with Wind/3DP instrument and the QTN spectroscopy technique on board STEREO A are finally compared, showing a good agreement between Wind and STEREO for additional verification.

2. Basics of the Method

The QTN method can be applied to measurements in frequency range above ion plasma frequency $\omega >> \omega_i \approx (m_e/m_i)^{1/2}\omega_p$ (where $\omega_p = \sqrt{n_e e^2/\epsilon_0 m_e}$) up to range of significant galactic radiation ($\sim$ few hundred kilohertz [*Zaslavsky et al.*, 2011]). In this range, the voltage spectral density measured at the terminals of an electric antenna in the solar wind consists of three different contributing noises: the electron quasi-thermal noise V^2_{qtn} due to the ambient electrons thermal motion, the proton noise V^2_p due to the protons thermal motion which is Doppler shifted by the solar wind bulk speed, and the electron shot noise V^2_{sn} due to electron impacts on the antenna. All three of these components are highly affected by antenna size and shape. Spectrum observed by the receiver is as follows:

$$V^2_{\mathrm{obs}} = \Gamma^2\left(V^2_{\mathrm{qtn}} + V^2_p + V^2_{\mathrm{sn}}\right) + V^2_{\mathrm{LFR}} \tag{1}$$

Here V^2_{LFR} is receiver internal noise, given by *Bougeret et al.* [2008], and Γ is attenuation factor due to capacitive coupling between the antennas and the receiver's mechanical/electrical structure. Namely, the antenna with impedance Z is connected to the receiver with a finite impedance Z_R containing "stray" or "base" capacitance C_b, and gain is defined as $\Gamma = C_{\mathrm{ant}}/(C_{\mathrm{ant}} + C_b)$. Base capacitance for STEREO/WAVES has been measured to be $C_b \approx 32$ pF [*Bale et al.*, 2008; *Zouganelis et al.*, 2010]. Value of antenna capacitance is a function of frequency, but it can be approximated by a constant factor at any frequency except at $\omega \sim \omega_p$. Actual value of the STEREO/WAVES antenna capacitance is measured by *Bale et al.* [2008] to be $\approx$ 63 pF for a monopole which should be equivalent to twice the capacitance of a dipole. This result is in accordance with formula for the reactance of a monopole antenna above an infinite ground plane [*Balanis*, 1997]. Also, the given value is in good agreement with approximation for $L_{\mathrm{ant}} << L_D$ (which is not always the case on STEREO) given by *Meyer-Vernet and Perche* [1989] to be

$$C_{\mathrm{ant}} = \frac{\pi\epsilon_0 L_{\mathrm{ant}}}{\lg\left(L_{\mathrm{ant}}/a_{\mathrm{ant}}\right) - 1} \approx 31.7\ \mathrm{pF} \tag{2}$$

for a wire dipole, where a_{ant} is the antenna radius. From here the receiver gain is given by

$$\Gamma = \frac{C_{\mathrm{ant}}}{C_{\mathrm{ant}} + C_b} \approx 0.49 \tag{3}$$

2.1. Electron Quasi-Thermal Noise

When a passive electric antenna is immersed in a stable plasma, the thermal motion of ambient particles produces electrostatic fluctuations, which can be adequately measured with a sensitive wave receiver connected to the wire dipole antenna.

If VDF of electrons is isotropic, then signal measured on the antenna terminals due to quasi-thermal noise is given as [*Chateau and Meyer-Vernet*, 1991] follows:

$$V_{\mathrm{qtn}}^2(\omega) = \frac{16 m_e \omega_p^2}{\pi \epsilon_0} \int_0^{+\infty} \frac{F(kL_{\mathrm{eff}}) B(k)}{k^2 |\epsilon_L|^2} \mathrm{d}k \tag{4}$$

In equation (4), k is the wave number, and L_{eff} is effective antenna length that takes into account the angle between antenna arms [*Meyer-Vernet and Perche*, 1989]. Since on STEREO we have 90° angle between the monopoles [*Bale et al.*, 2008], we have $L_{\mathrm{eff}} = \sin(\pi/4) L_{\mathrm{ant}}$ in the limit $L_{\mathrm{ant}} << L_D$. This value of L_{eff} is a rough approximation, but it can work well for STEREO since V_{qtn}^2 is only a small contribution to the power spectrum. Antenna response function for a wire dipole antenna $F(kL_{\mathrm{eff}})$ is given as follows:

$$F(x) = x^{-1} \left[Si(x) - \frac{1}{2} Si(2x) - \frac{2}{x} \sin^4 \frac{x}{2} \right] \tag{5}$$

where $Si(x)$ stands for the sine integral. Function $B(k)$ is defined in following way

$$B(k) = \frac{2\pi}{k} \int_{\omega/k}^{+\infty} v f(v) \mathrm{d}v \tag{6}$$

and longitudinal dielectric permittivity is

$$\epsilon_L = 1 + \frac{2\pi\omega_p^2}{k} \int_{-\infty}^{+\infty} \frac{v f(v)}{kv - \omega - i_0} \mathrm{d}v \tag{7}$$

All given components are determined by VDF of electrons. In free solar wind, since "kappa" (κ) VDF has been commonly observed [*Maksimović et al.*, 2005; *Štveràk et al.*, 2009], we choose to use the model of QTN spectrum for κ VDF, which is given in details by *Chateau and Meyer-Vernet* [1991] and *Le Chat et al.* [2009]. This kind of VDF is actually a generalized Lorentzian, power law distribution with higher percentage of suprathermal electrons as compared to the classic Maxwellian, and is defined as follows:

$$f(v) = \frac{\Gamma(\kappa+1)}{(\pi\kappa)^{3/2} v_0^3 \Gamma(\kappa - 1/2)} \frac{1}{\left(1 + \frac{v^2}{\kappa v_0^2}\right)^{\kappa+1}} \tag{8}$$

where $\Gamma(x)$ denotes the gamma function and v_0 is the thermal speed related to the kinetic temperature T_e as

$$v_0 = \left(\frac{2\kappa - 3}{\kappa} \frac{k_b T_e}{m_e} \right)^{0.5} \tag{9}$$

VDF is defined for $\kappa > 1.5$, and for $\kappa \to \infty$ it reduces to the Maxwellian distribution. It is convenient to define the average velocity as the first moment of the 3-D distribution [*Chateau and Meyer-Vernet*, 1991].

$$< v > = 2\sqrt{\frac{\kappa}{\pi}} \frac{\Gamma(\kappa - 1)}{\Gamma(\kappa - 0.5)} v_0 \tag{10}$$

which converges to Maxwellian value of $< v > = \sqrt{8 k_b T_e / \pi m_e}$ for very large values of κ index.

2.2. Proton Quasi-Thermal Noise

We estimate the proton contribution using the model developed by *Issautier et al.* [1999]. If the antenna is perpendicular to the solar wind velocity $\vec{v_{\mathrm{sw}}}$, which is an acceptable approximation for STEREO, the proton noise is given by

$$V_p^2(\omega) = \frac{(2 m_e k_b T_e^*)^{1/2}}{4\pi\epsilon_0 M} \int_0^{+\infty} \frac{y F_\perp(y L_{\mathrm{eff}}/L_D)}{(y^2 + 1 + \Omega^2)(y^2 + 1 + \Omega^2 + t)} \mathrm{d}y \tag{11}$$

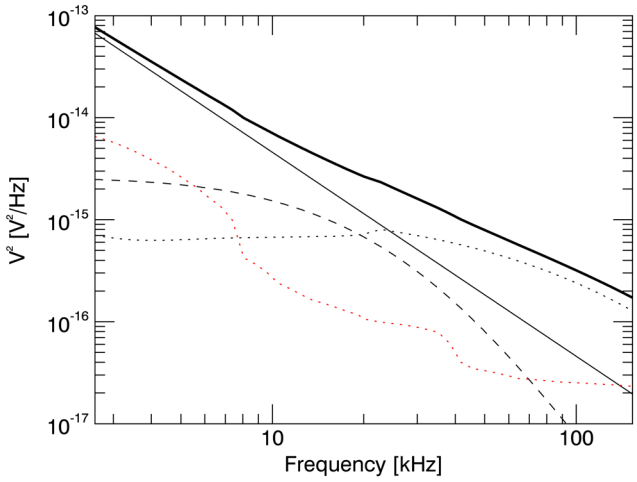

Figure 1. Theoretical spectrum of noise observed by STEREO. Shot noise is dominant (black line). Proton contribution is marked by dashed line and QTN by dotted line. LFR instrument noise is given by red dots. The thick solid line is the total of the noise components. Assumed conditions in the solar wind are as follows: $n = 5$ cm^{-3}, $T_e = 10$ eV, $\kappa = 4$, $v_{sw} = 340$ km/s, $T_p = 4.3$ eV, $f_p \approx 21$ kHz. Receiver gain is assumed to be $\Gamma \approx 0.5$.

where T_e^* is generalized electron temperature given as

$$T_e^* = \frac{m_e}{k_b < v^{-2} >} = \frac{2\kappa - 3}{2\kappa - 1} T_e \quad (12)$$

The generalized kinetic temperature is related to the local Debye length as $L_D = \sqrt{\epsilon_0 k_b T_e^* / e^2 n_e}$. In equation (11) we have $\Omega = \omega L_D / v_{sw}$, $t = T_e^*/T_p$, and $M = v_{sw}/v_0$ where T_p is proton temperature and $F_\perp$ is the antenna response function to a wavefield having cylindrical symmetry given by *Meyer-Vernet et al.* [1993] to be

$$F_\perp(x) = \frac{8}{x}\left[2\int_0^x J_0(t)dt - \int_0^{2x} J_0(t)dt + J_1(2x) - 2J_1(x)\right] \quad (13)$$

The proton noise spectrum is strongly Doppler shifted, so it can be observed far above the proton characteristic frequencies, which are in order of ω_i [*Issautier et al.*, 1996] and contributes significantly to the spectrum.

2.3. Electron Shot Noise

For $f < f_p$, shot noise on a wire dipole is approximated by *Meyer-Vernet* [1983] to be

$$V_{sn}^2 = 2e^2 N_{impact} |Z|^2 \quad (14)$$

where Z is the antenna impedance. Number of impacts on the antenna surface per unit time is given by

$$N_{impact} = j_e S_{ant} A \quad (15)$$

where $S_{ant} = 2\pi a_{ant} L_{ant}$ is the antenna surface and A is a correction factor due to the potential of the antenna (Appendix A). Flux of electrons from surrounding plasma is $j_e = n_e < v > /4$. The impedance of the antenna in an isotropic plasma can be well approximated by $Z = (i\omega C_{ant})^{-1}$ if real part of the antenna impedance R_{ant} is negligible comparing to its imaginary part. The condition for this so-called capacitively coupled regime is $\omega >> (R_{ant} C_{ant})^{-1}$ and holds for $\omega > 1$kHz on STEREO.

3. STEREO/WAVES Data Analysis

3.1. LFR Instrument

The STEREO/WAVES instrument uses three 6 m monopole antennas; each antenna is having an average radius of 1.15 cm [*Bale et al.*, 2008]. LFR [*Bougeret et al.*, 2008] is a digital spectral analyzer that produces voltage power in three 2-octave bands, covering frequency range from 2.5 to 160 kHz with spectral resolution $\delta f/f \approx 8.7\%$. Each one of the bands includes 16 logarithmically spaced frequency channels. Frequency range of LFR is actually the range of dominating electrostatic noise in the solar wind (see section 2). Time resolution of measurements is ≈ 38.5 s, and the signal is obtained by performing a Fourier transform of the voltage fluctuations.

Internal noise of the receiver [*Bougeret et al.*, 2008] is at least an order of magnitude below the measured power spectrum. On Figure 1 is shown the spectrum expected to be observed by LFR instrument for typical plasma parameters in free solar wind at 1 AU. Shot noise is dominant at low frequencies and gives the shape of the spectrum which is almost linear at logarithmic scale. However, other contributions cannot be neglected in the analysis since sum of the QTN and the proton noise becomes equal to the shot noise at $f \sim 0.6 f_p$. It is worth noting that the spectrum shown is valid only at frequency range where shot noise can be approximated by equation (14) (for $f < f_p$).

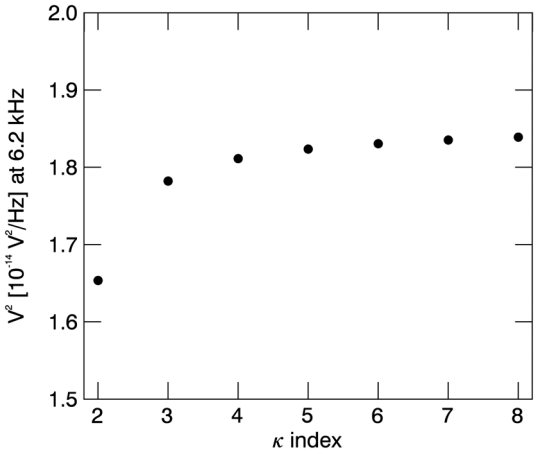

Figure 2. Level of the theoretical spectrum at 6.2 kHz for different values of κ index. Plasma parameters are $n_e = 7.39\,\mathrm{cm}^{-3}$, $T_e = 11$ eV, $v_{sw} = 349.1$ km/s, $n_p = 7.32\,\mathrm{cm}^{-3}$, $T_p = 6.5$ eV. Receiver gain is assumed to be $\Gamma \approx 0.5$. The spectrum level is nearly flat for $\kappa > 3$.

3.2. Data Analysis

QTN spectrum is a function of six independent parameters: electron and proton densities n_e and n_p, electron and proton kinetic temperatures T_e and T_p, solar wind bulk velocity v_{sw}, and κ index. In general, these parameters can be obtained separately by fitting the spectrum given in equation (1) [*Le Chat et al.*, 2011]. Unfortunately, on STEREO this is not possible, since short and thick antennas cause the shot noise to overwhelm all other contributions. Also, the condition $L_{\mathrm{eff}} < L_D$, valid for STEREO in the free solar wind, makes the plasma peak that is normally used for accurate estimation of electron density invisible. The almost linear shape of the spectrum (Figure 1) allows us to derive only one independent parameter. Consequently, we fitted the data with a single free parameter—the electron temperature, while other parameters were taken from PLASTIC instrument [*Galvin et al.*, 2008]. Electron density, not measured by PLASTIC, was approximated to be equal to the proton density plus an additional 8% due to presence of around 4% of α particles in free solar wind [*Matthias et al.*, 2001], which are also not detected by the proton analyzer.

On the other hand, the effective temperature obtained by application of the model to the data is slightly dependent of the value of "κ" index. This value needs to be assumed before data processing. The "true" value of κ in the solar wind may vary significantly depending on distance from the Sun [*Maksimović et al.*, 2005; *Štveràk et al.*, 2009] and solar wind speed [*Maksimović et al.*, 1997] and has been measured by various authors [e.g., see *Zouganelis*, 2008; *Le Chat et al.*, 2011]. Most of the authors evaluate $\kappa \approx 4 \pm 1$ in the slow wind at 1 AU, which is the position of STEREO. This parameter affects all three components of the spectrum (electron, proton, and shot noise) but, combined, κ value affects the power spectrum by less than 2% for $\kappa \geq 3$ in the case of STEREO. Figure 2 represents the level of the power spectrum at 6.2 kHz calculated using our model. Variation between the signal expected to be observed for $\kappa \geq 2$ (the range of commonly observed κ index at 1 AU) is smaller than 10%. In order to avoid multiple parameter fitting of the data set which is almost linear in logarithmic scale, we use the constant value of $\kappa = 4$ further on, as done by some previous authors. Error in measurement of T_e that is produced this way is less than 3%, being much less than uncertainties that originate from the instrument (section 3.3).

Since equation (14) only holds for $f < f_p$ [*Meyer-Vernet and Perche*, 1989], all the frequencies above 9.57 kHz have been excluded from the fitting process (only Band A of the LFR is used). This way, we consider only the part of a spectrum below the plasma frequency, and each spectrum is fitted using 16 frequency channels.

The main issue of the fitting procedure was filtering of measured spectra by quality and establishing criteria for their usability. Namely, as antennas on STEREO are not suitable for fine QTN spectrum measurements, measured spectra are very sensitive to any kind of "pollution" by dust impacts, Langmuir waves, etc., which can appear and cover the ubiquitous thermal noise. This kind of spectra are not taken into account since their usage is propensed to give some unrealistic and incorrect results during the massive fitting procedure applied to the entire STEREO database (9 years, until now, of data with ~40 s time resolution).

Spectra with dust impacts are completely excluded as unusable. They are fairly easy to recognize due to characteristic f^{-4} spectrum characteristic and very high intensities of signal [*Meyer-Vernet et al.*, 2009]. The reason for such high sensitivity of STEREO antennas to dust impacts, compared to other spacecraft, is very large antenna radius a_{ant} [*Pantellini et al.*, 2012], which causes the signal to be 4–5 orders of magnitude above the usual shot noise signal. These features were used by *Meyer-Vernet et al.* [2009] and *Le Chat et al.* [2013] to discover and study nanodust impacts on STEREO. Linear fitting of every spectrum is performed.

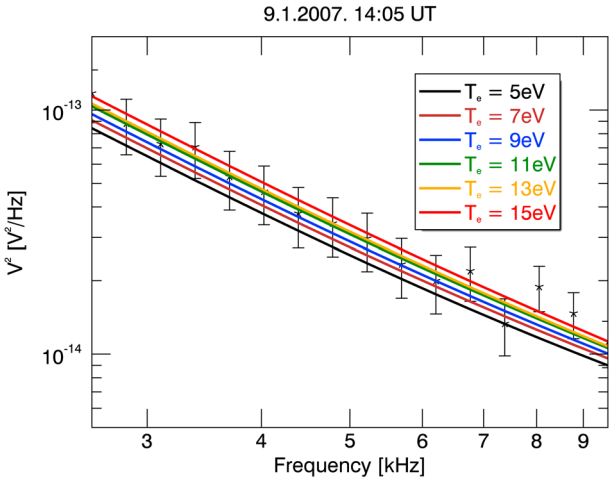

Figure 3. Example of LFR spectrum. Measured values are given by asterisks with marked error bars. Plasma parameters measured by Wind (section 4) for given time have the same values as in Figure 2, with $\kappa = 4$. Spectra calculated by using the model for multiple values of T_e are given in different colors.

If the slope obtained from linear fit $\lg f, \lg V^2$ is less than −1.8 for entire spectrum or less than −3 for first five data points (2.6–3.7 kHz), the spectrum is not taken into account. The reason for this treatment is the fact that signals caused by dust can manifest, in certain occasions, only at low frequencies.

3.3. Necessity of Averaging of the Results

The electron kinetic temperature measured by the model described in section 2 is very sensitive to the level of power spectrum measured by the receiver in the case of STEREO. Namely, for all three components (QTN, proton, and shot noise) the noise level is roughly scaled with $T_e^{0.5}$. This means that the value of measured T_e can vary significantly with any kind of fluctuations in measurements. Figure 3 illustrates this effect. It is noticeable that measurement errors of the LFR instrument [*Bougeret et al.*, 2008] cover very broad range of temperatures. This inevitably leads to very a big dispersion of the results.

In order to overcome this effect, averaging of results over certain time period needs to be performed. This way, the result of the measured electron temperature is given as an average value for the chosen period. To choose the time interval most suitable for time averaging, we compared temperature measurements using the technique described above to measurements performed by Wind. For this we use the same period which was used for the measurement of base capacitance by *Zouganelis et al.* [2010]. In Figure 4 of that paper is given a histogram of measured C_b values that also confirms existence of the strong fluctuations described here. Details of the comparison, as well as criteria used to determine the averaging time interval, are given in section 4.1.

Since, in the process of averaging, we assume that the true value of T_e does not change during the given time interval, value of the error bars is calculated as standard deviations of the mean value of the results during the averaging period $<\sigma> = \sigma/\sqrt{N}$, where N is number of measurements and σ is standard deviation of the measured T_e values during the time interval. As we neglect changes of the value of T_e during the given time interval, as well as error of each particular measurement, the values of the error bars can be (sometimes highly) underestimated.

4. Comparison With Wind

4.1. Real-Time Test and Averaging Intervals

Electron analyzers on both STEREO spacecraft are not functioning properly since launch [*Fedorov et al.*, 2011], and unfortunately, there is no data on thermal electrons at all, so that validity of the results cannot be confirmed in real time. In order to validate our results, we compared value of T_e derived by the model (section 2) to the one measured by Wind when STEREO B was positioned just behind it. Namely, during the observed day (9 January 2007), in the early phase of the STEREO mission, while STEREO B was performing its rotation around the Earth in preparation to start rotating around the Sun, it formed a straight line with the Sun and Wind, which was standardly located at L1 point at ~0.99 AU.

Unfortunately, during the selected period, there was no PLASTIC data, so all particle data necessary for the analysis are taken from Wind. For providing electron data on Wind, the Wind/WAVES thermal noise receiver [*Bougeret et al.*, 1995] plasma peak (clearly visible because of long and thin antennas) was used for a reference value of the electron density, since that is crucial for our obtaining of accurate electron parameters. Using n_e obtained this way, fits of VDF, as it is measured by Wind/3DP [*Lin et al.*, 1995], were performed. Some details of this procedure are given in *Pulupa et al.* [2014]. Finally, we applied the fitting procedure described

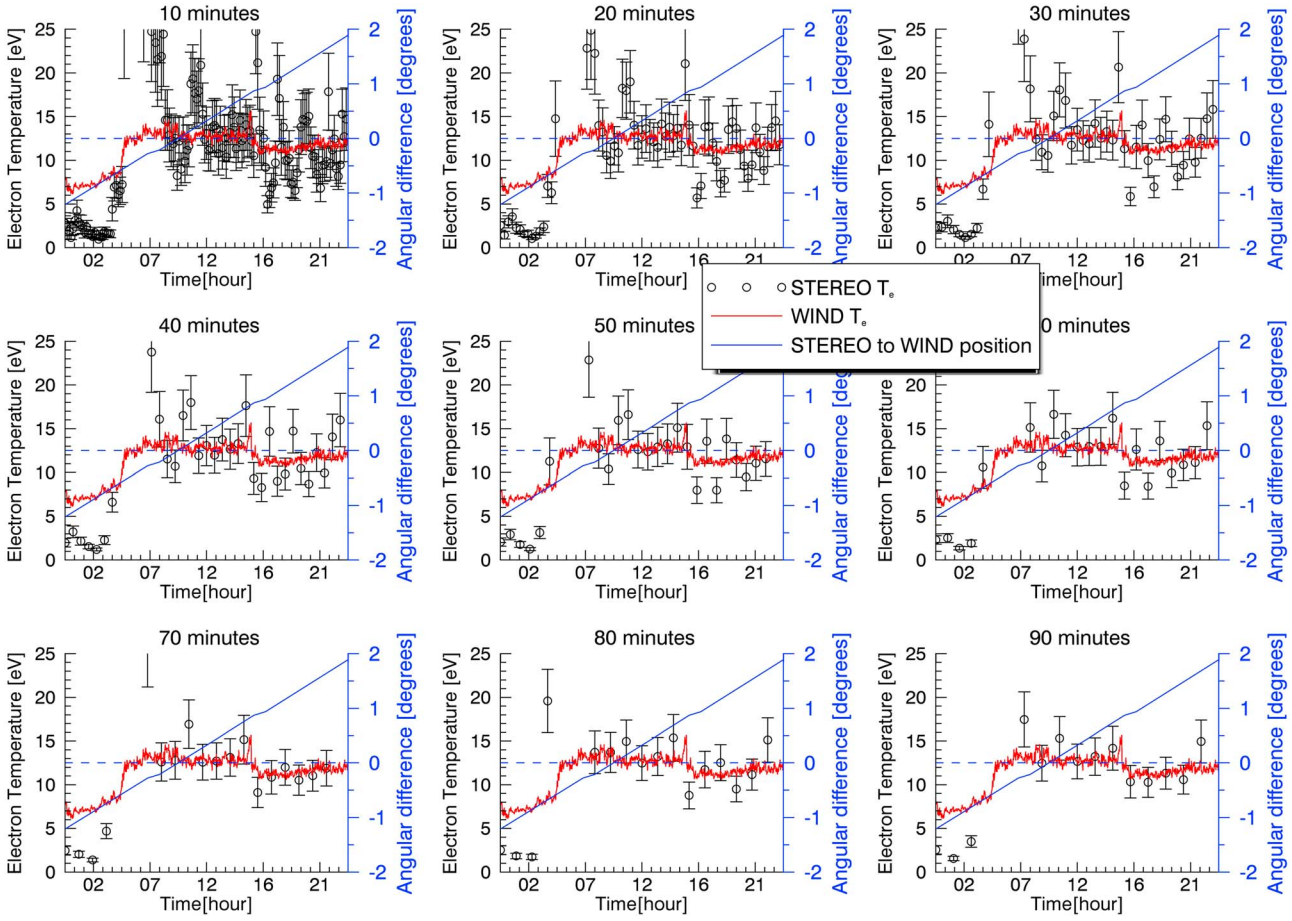

Figure 4. Electron temperature as measured by STEREO B/LFR on 9 January 2007 averaged over different time intervals (circles). T_e from Wind/3DP data used for comparison is given in red. Blue line stands for the angle between lines that connect Wind and the Sun and Wind and STEREO B.

in section 3.2, with parameters n_p and T_p measured by Wind/SWE [*Ogilvie et al.*, 1995], n_e and v_{sw} measured by Wind/3DP (as described above), and $\kappa = 4$. The only fitted parameter was electron temperature which is compared with T_e, also measured by Wind/3DP. Figure 4 presents the results of this comparison.

Electron temperatures from Wind and STEREO B are plotted, showing a good agreement when spacecraft are close to each other (the relative position is shown by the blue line). In this figure it can be noted that T_e is highly underestimated at the first part of the day (until 8 A.M). The reason for this is a very strong change of the electron density at Wind itself, as Wind/3DP measures $n_e \sim 25\ \mathrm{cm}^{-3}$ during this period, and we conclude that the electron densities did not have the same value for the two spacecraft. Namely, because of the conspicuous sensitivity of the model to the assumed electron density, the difference of parameters on Wind and STEREO can highly affect results of our test, giving unrealistic values. For this very reason, period before 8 A.M. of this particular day was not used for base capacitance measurement in the previous work of *Zouganelis et al.* [2010].

Choice of the time duration on which to perform averaging is a compromise between decrease of the statistical error (assuming that T_e does not change during the time interval) and time resolution of the results, so it needed to be chosen arbitrarily. In Figure 4 are represented multiple averaging times. Time statistical error decreases as number of averaged results (time interval) increases. On the other hand, electron temperature is not constant over time, and for longer time intervals results will have larger deviations, depending on how the true value of T_e varies. Consequently, the "optimal" time interval for averaging of results can be found using these two premises. From the test period shown in Figure 4 the 60 min time interval has been selected and used further on, since the uncertainties of the measured T_e do not decrease for longer averaging periods.

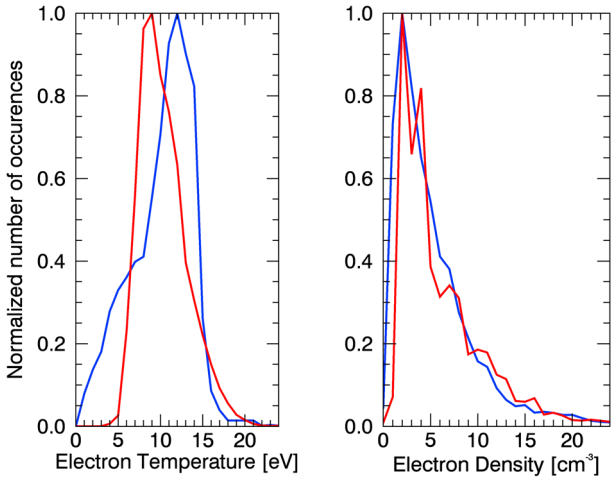

Figure 5. Histograms of electron density and temperature measured by Wind/3DP (red lines) and evaluated for STEREO (blue line) for 10 months during the year of 2007. Here as electron density is given the proton density measured by PLASTIC increased by 8% (section 3) and electron temperature is calculated by applying our model to the STEREO A/LFR data.

4.2. Processing a Large Data Set

For additional verification, all the STEREO A spectra from 10 months (March to December) in year of 2007 have been processed, and histogram plots were compared with Wind measurements. It is worth noting that around 85% of this period is covered by dust [*Zaslavsky et al.*, 2012], so number of spectra used from STEREO A is much smaller than number of those taken from Wind, but still enough to perform the statistics. Results are given in Figure 5. It is noticeable that PLASTIC gives more scattered values for proton density compared to well-calibrated Wind measurements. Although both histograms peak at the same value ($\approx 2\,\mathrm{cm}^{-3}$), values of n_p are, in general, underestimated by PLASTIC, but higher densities are measured more often than on Wind. Consequently, measured electron temperature is overestimated, and also, existence of low-temperature "tail" can be noticed. The source of this tail is due to measurements where overestimation of density is evident on PLASTIC. To confirm this statement, we made a "test" histogram (not shown here) where we exclude all measurements where $n_p > 5\,\mathrm{cm}^{-3}$. On this histogram, the low-temperature tails do not exist.

In order to verify the method, we compare histograms of $n_e\sqrt{T_e}$. Result is shown in Figure 6, and there is relatively good agreement between measurements from both spacecraft. "Dissipation" of results that originates from PLASTIC can also be noticed on this figure. Processing of PLASTIC data has been approached in different ways several times during the STEREO mission and, as soon as values of plasma density are updated, we will be able to provide reliable measurements of the electron temperature.

5. Summary and Conclusions

In this work, QTN spectroscopy has been accommodated for usage on STEREO spacecraft. Using LFR instrument measurements, we are able to provide, for the first time, a continuous survey of the electron temperature on both STEREO A and B, averaged on 1 h time period. Since characteristic plasma peak of QTN spectrum is not visible in the solar wind on STEREO, PLASTIC instrument data were used to approximate electron density, as well as to obtain information about proton density and temperature. The results were compared with Wind data. The test in real time, when STEREO B was close to Wind gives a good agreement between our method and Wind measurements, with ~20% uncertainties of the measured results. On the other hand, the 10 month histogram of T_e is highly dependent on n_p data from PLASTIC which itself does not agree with same sort of data from Wind. At this time,

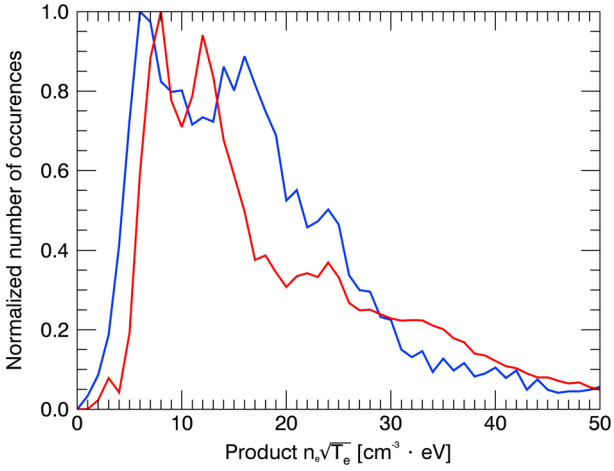

Figure 6. Histogram $n_e\sqrt{T_e}$ measured by Wind/3DP (red line) and STEREO (blue line) for the same data set as in Figure 5.

Table A1. Expressions for Correction of the Shot Noise Due To the Antenna Potential for Some Values of κ Index (Substitution $\eta = e\phi/k_bT_e$ Is Used)

κ	A
2	$\frac{1-(2\eta)^{3/2}}{1-2\eta}$
3	$\frac{9+6^{1/2}\eta^{3/2}(2\eta-5)}{(3-2\eta)^2}$
4	$\frac{-500+10^{1/2}\eta^{3/2}(175+12\eta(\eta-7))}{4(2\eta-5)^3}$
5	$\frac{19208+14^{1/2}\eta^{3/2}(-5145+2\eta(1323+10\eta(2\eta-27)))}{8(7-2\eta)^4}$

we are able to provide approximate values of $n_e\sqrt{T_e}$. In the future, as soon as PLASTIC data are updated, we will perform a complete study of the entire STEREO database to obtain electron temperature and make results available to the community.

Appendix A: Corrections due to Antenna Potential

In order to calculate the impact rate of the electrons, we use the method given by *Laframboise and Parker* [1973]. This method relies to the "orbit-limited" theory established by *Mott-Smith and Langmuir* [1926]. Here the method is applied to κ VDF in cylindrical geometry.

If we assume that plasma is collisionless and that the antenna potential ϕ is positive, then the total number of electrons that reach the antenna surface per unit time, given by equation (15), is evaluated as follows:

$$N_{\text{impact}} = n_e S_{\text{ant}} \frac{\Gamma(\kappa+1)}{\Gamma(\kappa-1/2)\pi^{3/2}\kappa^{3/2}v_0^3} \int_{\sqrt{\frac{2e\phi}{m_e}}}^{\infty} \mathrm{d}v \int_{-\pi/2}^{\pi/2} \mathrm{d}\theta \int_{-\infty}^{\infty} \mathrm{d}v_z \frac{v^2\cos\theta}{\left(1+\frac{v^2-\frac{2e\phi}{m_e}+v_z^2}{\kappa v_0^2}\right)^{\kappa+1}} \tag{A1}$$

where v and v_z are radial and tangential velocity components with respect to the axis of the antenna. From here we make substitutions $x = v\kappa^{-1/2}v_0^{-1}$ and $y = v_z\kappa^{-1/2}v_0^{-1}$ and obtain

$$A = \frac{N_{\text{impact}}}{j_e S_{\text{ant}}} = \frac{4\Gamma(\kappa+1/2)}{\pi^{1/2}\Gamma(\kappa-1)} \int_{\eta_\kappa^{1/2}}^{\infty} \frac{x^2\mathrm{d}x}{(1+x^2-\eta_\kappa)^{\kappa+1/2}} \tag{A2}$$

where

$$\eta_\kappa = \frac{2}{2\kappa-3}\frac{e\phi}{k_bT_e} \tag{A3}$$

Integral in equation (A2) can be represented in terms of regularized hypergeometric function as follows:

$$A = 2\pi^{-1/2}\Gamma(\kappa+1/2)[\Gamma(\kappa)]^{-1}\eta_\kappa^{1-\kappa}{}_2\bar{F}_1\left(\kappa-1,\kappa+1/2,\kappa,1-\eta_\kappa^{-1}\right) \tag{A4}$$

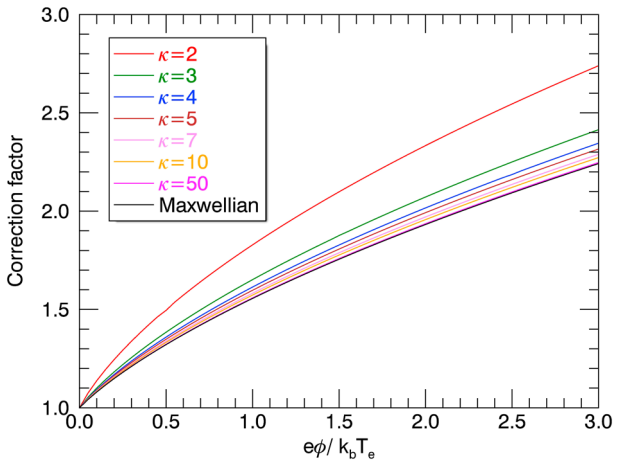

Figure A1. Shot noise correction factor due to antenna potential for different values of κ index. Black line is the result given by *Mott-Smith and Langmuir* [1926] and *Laframboise and Parker* [1973] for Maxwellian electrons.

and can be solved analytically for integer values of κ. Solutions are given in Table A1 and Figure A1. It can be noticed that values of factor A are reasonably higher for the plasmas with κ VDFs then for the Maxwellian plasmas of the same temperature.

The antenna potential ϕ in cylindrical geometry is derived directly from condition that current produced by photoelectrons escaping from the antenna potential well and by electrons being collected from the surrounding plasma are balanced. Namely, in the solar wind at 1 AU, the photoelectron escape flux is much larger than the electron flux of surrounding plasma if the antenna is at plasma potential, so the potential

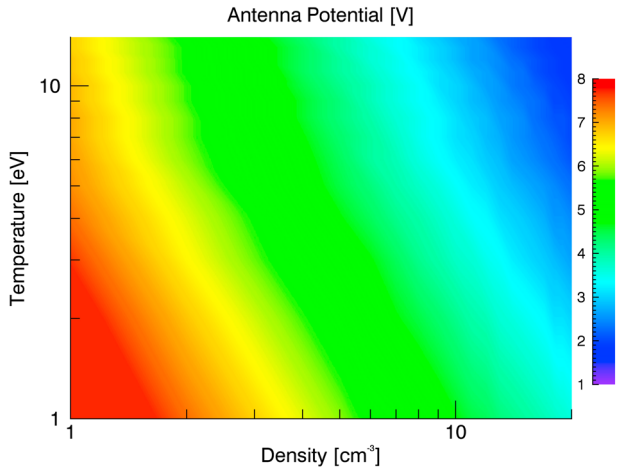

Figure A2. Dependence on plasma parameters for the potential of the antenna. For this example, $\kappa = 4$ is assumed.

becomes positive to prevent the escape of too many photoelectrons. If the spectrum of the emitted photoelectrons is Maxwellian, we have for the current balance equation:

$$S_{\perp} j_{\mathrm{ph}} e^{-\frac{e\phi}{k_b T_{\mathrm{ph}}}} = S_{\mathrm{ant}} j_e A \qquad \text{(A5)}$$

Here $S_{\perp}$ is sunlight surface of the antenna. The *X* and *Y* monopoles are placed on the anti-Sun side of the spacecraft and inclined by ~125° and *Z* monopole by ~145° to the Sun-spacecraft direction, which gives approximate relations $S_{\mathrm{ant}}/S_{\perp_x} \approx 4.41$, $S_{\mathrm{ant}}/S_{\perp_y} \approx 3.84$, and $S_{\mathrm{ant}}/S_{\perp_z} \approx 6.19$ [*Kellogg et al.*, 2009].

In equation (A5), j_{ph} is photoelectron flux at zero antenna potential which depends only on properties of the surface material, and T_{ph} is temperature of photoelectrons. These values have been calculated and measured by many authors [e.g., see *Escoubet et al.*, 1997; *Scudder et al.*, 2000; *Pedersen et al.*, 2008] for many spacecraft and antenna covers and geometries. It has been evaluated to be $j_{\mathrm{ph}} \sim 1-5 \cdot 10^{14} \mathrm{m}^2\,\mathrm{s}^{-1}$ and $T_{ph} \approx 2-2.7$ eV for the antennas and $T_{ph} \approx 3$ eV [*Henri et al.*, 2011] for spacecraft covers. Here we use values $j_{\mathrm{ph}} = 1 \cdot 10^{14} \mathrm{m}^2\,\mathrm{s}^{-1}$ and $T_{\mathrm{ph}} = 2$ eV, which are just barely in range of the results given by previous authors and are also lower then the ones obtained in laboratory measurements for BeCu antennas [e.g., see *Spencer*, 1975]. Namely, in the space, these parameters are modified by both secondary emission of electrons (which has been neglected in our calculations) and changes in the work function of the surface due to impurities of the material. This applies that the exact values of the photoelectron parameters are unknown and need to be chosen arbitrarily. We use the values given here, as this choice does not seem to imply any systematic error in our measurements of T_e in the test described in section 4.1.

Antenna potential ϕ has been calculated for wide range of electron densities and temperatures and is given in Figure A2. For conditions of quiet solar wind ($n_e \approx 2-10\,\mathrm{cm}^{-3}$, $T_e \sim 10-15$ eV) value the potential is $\phi \approx 3-8$ V. This produces the correction to the electron impact rate (equation (15)) and, consequently, the shot noise for a factor of $A \approx 1.3-1.6$, but for lower temperatures, usually observed in some coronal mass ejections, it can increase up to 50% of its initial value and highly affect measured results.

Acknowledgments
The authors are grateful to the Ministry of Education, Science and Technological Development of Republic of Serbia for financing the projects ON176002. The Wind/SWE proton moments data were obtained freely from the NASA Coordinated Data Analysis Web (http://cdaweb.gsfc.nasa.gov/), while Wind/3DP and STEREO/LFR instrument data are available on CNES Plasma Physics Data Centre (http://cdpp.eu/). Thanks to the two reviewers for their constructive comments and helpful suggestions on an earlier version of the manuscript.

References

Balanis, C. A. (1997), *Antenna Theory: Analysis and Design*, Wiley, New York.
Bale, S. D., et al. (2008), The electric antennas for the STEREO/WAVES experiment, *Space Sci. Rev.*, *136*, 529–547.
Bougeret, J. L., et al. (1995), Waves: The radio and plasma wave investigation on the Wind spacecraft, *Space Sci. Rev.*, *71*, 231–265.
Bougeret, J. L., et al. (2008), S/WAVES: The radio and plasma wave investigation on the STEREO mission, *Space Sci. Rev.*, *136*, 487–528.
Chateau, Y. F., and N. Meyer-Vernet (1991), Electrostatic noise in non-maxwellian plasmas: Generic properties and "kappa" distributions, *J. Geophys. Res.*, *96*, 5825–5836.
Escoubet, C. P., A. Pedersen, and R. Schmidt (1997), Density in the magnetosphere inferred from ISEE 1 spacecraft potential, *J. Geophys. Res.*, *102*, 17,595–17,609.
Fedorov, A., A. Opitz, J. A. Sauvaud, J. G. Luhmann, D. Curtis, and D. Larson (2011), The impact Solar Wind Electron Analyzer (SWEA): Reconstruction of the SWEA transmission function by numerical simulation and data analysis, *Space Sci. Rev.*, *161*, 49–62.
Galvin, A., et al. (2008), The Plasma and Suprathermal Ion Composition (PLASTIC) investigation on the STEREO observatories, *Space Sci. Rev.*, *136*, 487–528.
Henri, P., N. Meyer-Vernet, C. Briand, and S. Donato (2011), Observations of Langmuir ponderomotive effects using the solar terrestrial relations observatory spacecraft as a density probe, *Phys. Plasmas*, *18*, 82308.
Issautier, K., N. Meyer-Vernet, M. Moncuquet, and S. Hoang (1996), A novel method to measure the solar wind speed, *Geophys. Res. Lett.*, *23*, 1649–1652.
Issautier, K., N. Meyer-Vernet, M. Moncuquet, and S. Hoang (1999), Quasi-thermal noise in a drifting plasma: Theory and application to solar wind diagnostic on Ulysses, *J. Geophys. Res.*, *104*, 6691–6704.
Kellogg, P. J., K. Goetz, S. J. Monson, S. D. Bale, M. J. Reiner, and M. Maksimović (2009), Plasma wave measurements with STEREO S/WAVES: Calibration, potential model, and preliminary results, *J. Geophys. Res.*, *114*, A02107, doi:10.1029/2008JA013566.
Laframboise, J. G., and L. W. Parker (1973), Probe design for orbit-limited current collection, *Phys. Fluids*, *16*, 629–636.
Le Chat, G., K. Issautier, N. Meyer-Vernet, I. Zouganelis, M. Maksimović, and M. Moncuquet (2009), Quasi-thermal noise in space plasma: "Kappa" distributions, *Phys. Plasmas*, *16*, 102903.

Le Chat, G., K. Issautier, N. Meyer-Vernet, and S. Hoang (2011), Large-scale variation of solar wind electron properties from quasi-thermal noise spectroscopy: Ulysses measurements, *Sol. Phys.*, *271*, 141–148.
Le Chat, G., A. Zaslavsky, N. Meyer-Vernet, K. Issautier, S. Belheouane, I. Zouganelis, S. D. Bale, and J. C. Kasper (2013), Interplanetary nanodust detection by the solar terrestrial relations observatory/waves low frequency receiver, *Sol. Phys.*, *286*, 549–559.
Lin, R. P., et al. (1995), A three-dimensional plasma and energetic particle investigation for the Wind spacecraft, *Space Sci. Rev.*, *71*, 125–153.
Maksimović, M., V. Pierrard, and P. Riley (1997), Ulysses electron distributions fitted with kappa functions, *Geophys. Res. Lett.*, *9*, 1151–1154.
Maksimović, M., I. Zouganelis, J. Y. Chaufray, K. Issautier, E. E. Scime, J. E. Littleton, E. Marsch, D. J. McComas, C. Salem, R. P. Lin, and H. Elliot (2005), Radial evolution of the electron distribution functions in the fast solar wind between 0.3 and 1.5 AU, *J. Geophys. Res.*, *110*, A09104, doi:10.1029/2005JA011119.
Matthias, A. R., A. J. Lazarus, and J. T. Steinberg (2001), The solar wind helium abundance: Variation with wind speed and the solar cycle, *Geophys. Res. Lett.*, *136*, 2767–2770.
Meyer-Vernet, N. (1979), On natural noises detected by antennas in plasmas, *J. Geophys. Res.*, *94*, 2405–2415.
Meyer-Vernet, N. (1983), Quasi-thermal noise correction due to particle impacts of emission, *J. Geophys. Res.*, *88*, 8081–8093.
Meyer-Vernet, N. (1994), On thermal noise "temperature" in an anisotropic plasma, *Geophys. Res. Lett.*, *21*, 397–400.
Meyer-Vernet, N., and C. Perche (1989), Tool kit for antennae and thermal noise near the plasma frequency, *J. Geophys. Res.*, *94*, 2405–2415.
Meyer-Vernet, N., S. Hoang, and M. Moncuquet (1993), Bernstein waves in the Io plasma torus: A novel kind of electron temperature sensor, *J. Geophys. Res.*, *98*, 21,163–21,176.
Meyer-Vernet, N., M. Maksimović, A. Czechowski, I. Mann, I. Zouganelis, K. Goetz, M. L. Kaiser, O. C. St Cyr, J. L. Bougeret, and S. D. Bale (2009), Dust detection by the wave instrument on STEREO: Nanoparticles picked up by the solar wind?, *Sol. Phys.*, *256*, 463–474.
Mott-Smith, H. M., and I. Langmuir (1926), The theory of collectors in gaseous discharges, *Phys. Rev.*, *28*, 727–763.
Ogilvie, K. W., et al. (1995), SWE, A comprehensive plasma instrument for the Wind spacecraft, *Space Sci. Rev.*, *71*, 55–77.
Pantellini, F., N. Meyer-Vernet, S. Belheouane, and A. Zaslavsky (2012), Nano dust impacts on spacecraft and boom antenna charging, *Astrophys. Space Sci.*, *341*, 309–314.
Pedersen, A., et al. (2008), Electron density estimations derived from spacecraft potential measurements on cluster in tenuous plasma regions, *J. Geophys. Res.*, *113*, A07S33, doi:10.1029/2007JA012636.
Pulupa, M., S. D. Bale, C. Salem, and K. Horaites (2014), Spin-modulated spacecraft floating potential: Observations and effects on electron moments, *J. Geophys. Res. Space Physics*, *119*, 647–657, doi:10.1002/2013JA019359.
Scudder, J. D., X. Cao, and F. S. Mozer (2000), Photoemission current-spacecraft voltage relation: Key to routine, quantitative low-energy plasma measurements, *J. Geophys. Res.*, *105*, 21,281–21,294.
Spencer, W. T. (1975), Photoelectron emission analysis of surface elements of the International Sun Earth Explorer, Open File Rep. NAS5-20592, Avco Systems Division, Wilmington, Mass.
Štveràk, S., M. Maksimović, P. Trávníček, E. Marsch, A. N. Fazakerley, and E. E. Scime (2009), Radial evolution of nonthermal electron populations in the low-latitude solar wind: Helios, Cluster, and Ulysses Observations, *J. Geophys. Res.*, *114*, A05104, doi:10.1029/2008JA013883.
Zaslavsky, A., N. Meyer-Vernet, S. Hoang, M. Maksimović, and S. D. Bale (2011), On the antenna calibration of space radio instruments using the galactic background: General formulas and application to STEREO/WAVES, *Radio Sci.*, *46*, RS2008, doi:10.1029/2010RS004464.
Zaslavsky, A., et al. (2012), Interplanetary dust detection by radio antennas: Mass calibration and fluxes measured by STEREO/WAVES, *J. Geophys. Res.*, *117*, A05102, doi:10.1029/2011JA017480.
Zouganelis, I. (2008), Measuring suprathermal electron parameters in space plasmas: Implementation of the quasi-thermal noise spectroscopy with kappa distributions using in situ Ulysses/URAP radio measurements in the solar wind, *J. Geophys. Res.*, *113*, A08111, doi:10.1029/2007JA012979.
Zouganelis, I., M. Maksimović, N. Meyer-Vernet, S. D. Bale, J. P. Eastwood, A. Zaslavsky, M. Dekkali, K. Goetz, and M. L. Kaiser (2010), Measurements of stray antenna capacitance in the STEREO/WAVES instrument: Comparison of the measured voltage spectrum with an antenna electron shot noise model, *Radio Sci.*, *45*, 1005–1009, doi:10.1029/2009RS004194.

Erratum

In the originally published version of this article, a factor of 2 was missing from equation (14); equation (A4) was only partially correct and worked only under a certain range of parameters; and a reference and its citation in the text were incomplete. These errors have since been corrected, and this version may be considered the authoritative version of record.